ACS OMEGA

http://pubs.acs.org/journal/acsodf

Article

Synthesis and Characterization of 1*H*-Imidazole-4,5-dicarboxylic Acid-Functionalized Silver Nanoparticles: Dual Colorimetric Sensors of Zn^{2+} and Homocysteine

Palash Mondal* and Jeffery L. Yarger*

Cite This: *ACS Omega* 2022, 7, 33423−33431

Read Online

ACCESS | Metrics & More | Article Recommendations | Supporting Information

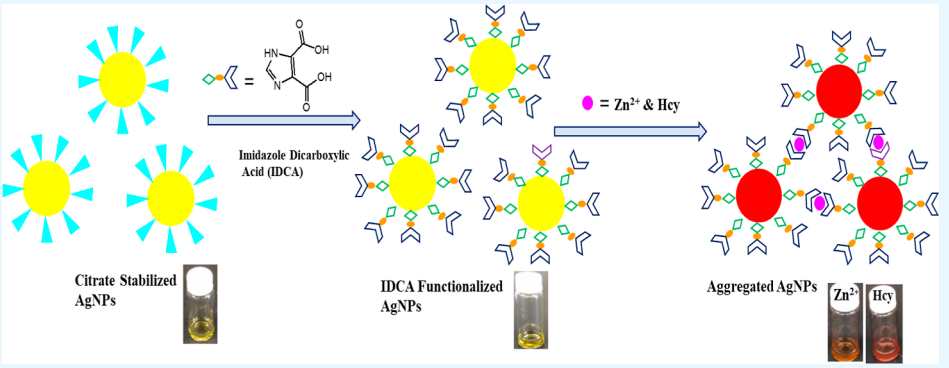

ABSTRACT: A colorimetric assay has been developed for Zn^{2+} and homocysteine (Hcy) detection using functionalized silver nanoparticles (AgNPs). AgNPs have been synthesized using silver nitrate, where sodium citrate is used as a stabilizing agent and $NaBH_4$ as a reducing agent. Then, the nanoparticles (citrate@AgNPs) were functionalized with 1*H*-imidazole-4,5-dicarboxylic acid (IDCA). UV−visible and FTIR spectra suggested that IDCA was functionalized on the surface of citrate@AgNPs through the N atom of the imidazole ring. The IDCA-functionalized silver nanoparticles (IDCA@AgNPs) simultaneously detected Zn^{2+} and Hcy from aqueous solution and showed different responses to the two analytes (Zn^{2+} and Hcy) based on the aggregation-induced color change of IDCA@AgNPs. They showed the color change from yellow to red, which was easily discriminated by visual inspection as well as UV−visible spectroscopy. The surface plasmon resonance absorbance values of Zn^{2+} and Hcy are 485 and 512 nm, respectively, when Zn^{2+} and Hcy react with IDCA@AgNPs. IDCA@AgNPs showed linearity with Zn^{2+} and Hcy concentrations, with the detection limit of 2.38 μM and 0.54 nM, respectively (S/N = 3). The IDCA@AgNPs showed excellent selectivity toward Zn^{2+} and Hcy compared to the different metal ions and amino acids, respectively. Optimal detection was achieved toward Zn^{2+} and Hcy in the pH range 3−10. In addition, IDCA@AgNPs were used to detect Zn^{2+} and Hcy from lake water, showing low interference.

1. INTRODUCTION

Zinc is the second most abundant transition element after iron, which participates in various aspects in biological metabolism. It plays various roles in the synthetic routes within cells,[1] normal growth of human body,[2] and normal brain function.[3] It is normally nontoxic, but uptake by humans due to high environmental concentrations of Zn^{2+} ion causes pulmonary manifestations, fever, chills, and gastroenteritis. Thus, the determination of trace amounts of Zn^{2+} ion is currently of great interest in medical sciences as well as environmental monitoring.

On the other hand, Hcy is a sulfur-containing amino acid in which a free −SH group is present as in cysteine, and Hcy is the intermediate formed during the conversion of methionine to cysteine. Free Hcy is not available naturally as it exists in plasma, in disulfide form as well as in protein-bound form. Therefore, it is complicated to determine the total Hcy after the reduction of disulfide. The normal concentration of Hcy in plasma ranges from 5 to 15 μM. The condition when the level of Hcy is above 15 μM is defined as hyperhomocysteinemia. High plasma levels of Hcy are associated with several diseases such as cardiovascular disease,[4] Alzheimer's disease,[5] neural tube defects,[6] and osteoporosis.[7] Hence, the determination of Hcy in plasma or protein is highly important.

Currently, there are common techniques employed for the detection of Hcy or Zn^{2+}, such as atomic absorption spectroscopy (AAS),[8] fluorescence,[9] electrochemical meth-

Received: July 2, 2022
Accepted: August 26, 2022
Published: September 7, 2022

https://doi.org/10.1021/acsomega.2c04165
ACS Omega 2022, 7, 33423−33431

Scheme 1. Synthesis of (a) Citrate@AgNPs and (b) IDCA@AgNPs after Centrifugation for 24 h and 60 °C

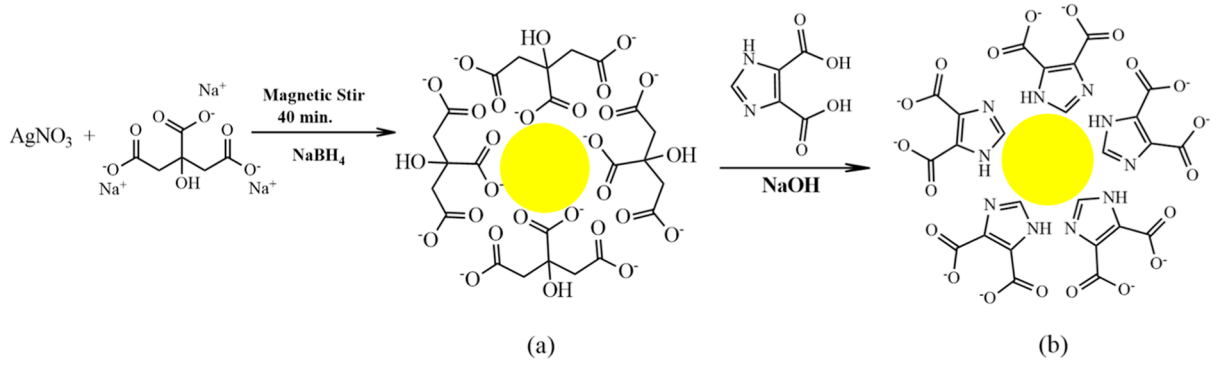

ods,[10] inductively coupled plasma mass spectrometry (ICP–MS),[11,12] and isotopic dilution mass spectrometry,[13,14] which provide sensitive, selective, and reproducible results, but they typically require expensive and sophisticated instruments, highly expensive that they are unsuitable for on-site analyses.

To contrast the abovementioned laboratory techniques, nanoparticle-based colorimetric sensors provide low-cost, simple monitoring and visual observation.[15] Among the various metallic nanoparticles, AgNPs are one of the most important other than gold nanoparticles due to the greater molar extinction coefficient (100-fold greater compared to gold), which improves the visibility and sensitivity when using absorption spectroscopy. Ihsan et al.[16] reported the synthesis of biologically synthesized colorimetric assay for selective determination of Zn^{2+} but not clearly study the selectivity test. Level-free silver nanoparticles were synthesized by K.-B. Lee and his co-worker[17] who reported the selective detection of Zn^{2+} but not in the presence of different pH of the medium. Karthiga and Anthony[18] reported the green synthesis of silver nanoparticles using leaf extracts for the determination of metal cations (Hg^{2+}, Pb^{2+}, Zn^{2+}, and Co^{3+}) over a wide range of pH. Furthermore, some reports were found using functionalized gold nanoparticles[19,20] for the colorimetric detection of Zn^{2+}. To the best of our knowledge, very few reports were found for the determination of Zn^{2+} ion using metallic nanoparticles, especially AgNPs and AuNPs. Therefore, there is enough scope to develop colorimetric sensors using AgNPs. On the other hand, a simple, portable detection method is really a challenge for the determination of Hcy from aqueous solution. Leesutthiphonchai et al.[21] reported the selective determination of Hcy levels in human plasma using a silver nanoparticle-based colorimetric assay. Uehara reported[22] the colorimetric assay of Hcy using gold nanoparticles conjugated with thermoresponsive copolymers. Thus, there are very few reports on the colorimetric sensing of Hcy using functionalized metallic nanoparticles.

Recently, almost all surface modifications of AgNPs are based on Ag–thiol interactions.[23,24] Because of the strong binding affinity between Ag and the sulfur atom of the ligands to produce Ag–S covalent bonds,[25] undesirable aggregations are expected during the modification and centrifugation separation steps. The stability of AgNPs is really a challenge for the long-term. In the present study, we report IDCA-functionalized AgNPs from the as-prepared citrate-capped AgNPs; as the N donors of IDCA have stronger affinity with AgNPs compared to the carboxyl group[26] without involving any complicated surface modification and tedious separation/purification processes, we envision that the IDCA-functionalized AgNPs might be suitable for the development of a highly selective and sensitive assay for the colorimetric dual sensing of Zn^{2+} and Hcy from aqueous solution.

2. SYNTHESIS OF FUNCTIONALIZED SILVER NANOPARTICLES

Silver nanoparticles (AgNPs) were prepared using $NaBH_4$ as a reducing agent and sodium citrate as a stabilizer according to a previously reported method with slight modifications.[27,28] Sodium citrate solution (10 mL, 50 mM) was added into a conical flask (500 mL), which contained silver nitrate solution (250 mL, 0.25 mM), under vigorous stirring for 40 min. Then, $NaBH_4$ (10 mL, 25 mM) was slowly added to the above solution at room temperature and stirred for 1 h. The dark colloidal solution changed to yellow, signifying the formation of citrate-capped AgNPs (Scheme 1a). To modify the surface of citrate-capped AgNPs, 100 mL of the as-prepared AgNP solution was taken in a 250 mL conical flask. Then, 0.078 g (0.5 mM) of 1*H*-imidazole-4,5-dicarboxylic acid (IDCA) (0.50 mM) was taken in 1 mM NaOH solution (10 mL, pH = 7.54) and added to the as-prepared 100 mL citrate@AgNP solution. Then, the mixture was stirred for 24 h at 60 °C, and the solution was cooled to room temperature. The IDCA@AgNPs (Scheme 1b) were obtained through centrifugation (25 min, 15,000 rpm) after removing the excess NaOH, IDCA, and citrate.

3. RESULTS AND DISCUSSION

3.1. Characterizations. Silver nanoparticles were prepared with citrate as the stabilizer and sodium borohydride as the reducing agent for $AgNO_3$. IDCA was added to the AgNP solution for surface functionalization. The UV–visible absorption spectra of citrate@AgNPs and IDCA@AgNPs are shown in Figure 1a,b. In Figure 1b,a slight red shift is observed from 393 to 397 nm, indicating that IDCA was modified on the surface of AuNPs as compared to that of the unmodified citrate@AgNPs. Moreover, we carried out control experiments using the citrate@AgNPs, which did not show any response to 50 μM Zn^{2+} and 1 μM of Hcy (Figure S1, Supporting Information). These results proved that the IDCA@AgNPs have sensing function in contrast to the citrate@AgNPs. Upon the addition of 50 μM Zn^{2+} or 1 μM Hcy to IDCA@AgNP solution, its color readily changes from yellow to red, due to the binding of Zn^{2+} or Hcy with IDCA, decreasing the distance of AgNPs, yielding both a substantial shift in the plasmon band energy to a longer wavelength and a yellow-to-red color change (Figure 1c,d).

https://doi.org/10.1021/acsomega.2c04165
ACS Omega 2022, 7, 33423–33431

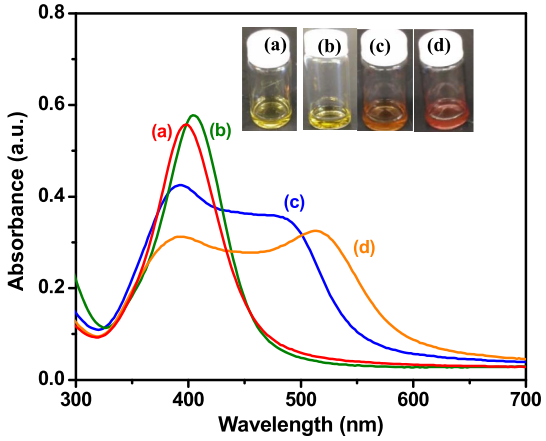

Figure 1. UV−vis spectra and photographic images (insert) of (a) citrate@AgNPs, (b) AgNPs@IDCA, (c) AgNPs@IDCA-Zn^{2+}, and (d) AgNPs@IDCA-Hcy.

To understand the nature of binding mode by IDCA on AgNP surfaces, we studied the FTIR spectra. The FTIR spectra of citrate@AgNPs and IDCA@AgNPs are shown in Figure 2. It is evident from Figure 2a that the characteristic

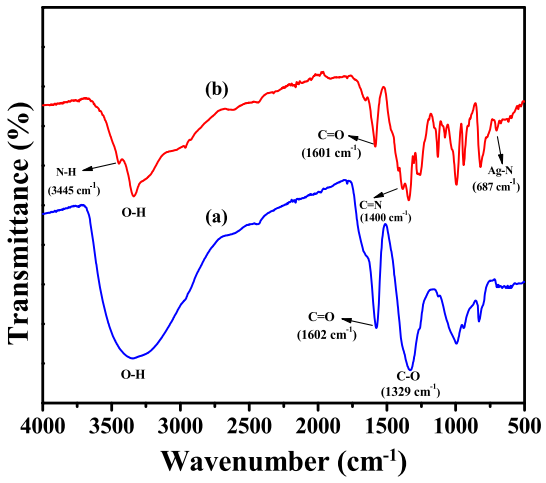

Figure 2. FTIR spectra of (a) citrate@AgNPs and (b) IDCA@AgNPs.

peaks of citrate@AgNPs are at 1600 cm^{-1} (υ_{as}, C═O) and 1329 cm^{-1} (υ_{s}, C−O), and a broad peak is around 3200−3420 cm^{-1} (O−H). The FTIR spectra of IDCA@AgNPs (Figure 2b) are similar to those of citrate@AgNPs. However, the difference is due to the appearance of two new peaks at 1400 cm^{-1} (C═N) and 3445 cm^{-1} (N−H stretching). These two new peaks are the characteristic peaks of the imidazole group in IDCA@AgNPs. Another new peak is present at 687 cm^{-1}, which is due to the Ag−N bond,[29] and this peak is absent in citrate@AgNPs (Figure 2a). Thus, FTIR and UV−vis spectra clearly confirmed that the IDCA ligand functionalized with the citrate@AgNP surface through the N atom of the imidazole ring of IDCA.

In order to confirm the morphology and size, we performed the dynamic light scattering (DLS) and transmission electron microscopy (TEM) analyses of citrate@AgNPs. The particle sizes of citrate@AgNPs ranged from 6 to 25 nm, and most of the particle sizes fell in the range of 8−15 nm, as evident from DLS (Figure 3a′), which is similar to the size distribution observed in the TEM images (Figure 3a). The DLS study and TEM are also performed for IDCA@AgNPs after the modification of citrate@AgNP surfaces. The particle sizes of IDCA@AgNPs ranged from 6 to 28 nm, and most of the particle sizes fell in the range of 9−21 nm, as evident from DLS (Figure 3b′), which is similar to the size distribution observed in TEM images (Figure 3b). The HRTEM images display the evidence of Zn^{2+}- and Hcy-induced aggregation of IDCA@AgNPs, as shown in Figure 3c,d, and their corresponding size distribution was also characterized by DLS (Figure 3c′,d′). With the addition of Zn^{2+}, the particle sizes ranged from 15 to 125 nm, and most of the particle sizes fell in the range of 25−80 nm, which is similar to the size distribution trends observed in the TEM images (Figure 3c). This observation indicated that Zn^{2+} induced the aggregation of IDCA@AgNPs. Similarly, with the addition of Hcy, the particle sizes ranged from 30 to 150 nm, and most of the particle sizes fell in the range of 40−90 nm. Thus, IDCA@AgNPs aggregate after binding with Hcy. The color change of AgNPs is highly sensitive to the size, shape, capping agents, medium refractive index, as well as the aggregation state of AgNPs.[30] Thus, change of color means variation of the size of AgNPs. When ligands as well as metal ions bind with AgNPs, "interparticle cross-linking mechanism"[31] occurs, resulting in the variation of color as well as size. When IDCA@AgNPs bind with Zn^{2+} and Hcy, resulting in the aggregation of AgNPs, various size ranges of particles were observed.

3.2. Influence of pH on IDCA@AgNPs. To investigate the pH range in which the IDCA@AgNPs can effectively detect Zn^{2+} or Hcy, a pH titration was carried out. The effect of pH on the absorption band of IDCA@AgNPs is shown in Figure S2 (Supporting Information), showing the stability of the prepared IDCA@AgNPs with respect to different pH values of the solution. From Figure S2, it is evident that the prepared IDCA@AgNPs are stable in the pH range from 3 to 10, but they are unstable and aggregated when pH > 10 or pH < 3. This is due to the chemical changes taking place in the IDCA@AgNP solution in the surroundings of particles; at pH < 3, all carboxylates are protonated, so the particles aggregate, whereas at pH > 10, the carboxyl groups of IDCA remain deprotonated and the hydroxyl groups in the solution can overwhelm the surface of AgNPs, which also reflect in the corresponding color of IDCA@AgNPs (Figure S2, Top). Therefore, for the monitoring of Zn^{2+} ion or Hcy, the pH range 3−10 is suitable and used. The pH of the mother solution (IDCA@AgNPs) was adjusted using phosphate-buffered saline (PBS), and the pH was around 5.4. We studied the pH for the determination of Zn^{2+} ion, and it is shown in Figure 4a. The suitable pH for the detection of Zn^{2+} ion is the range of 4−10, and the color of the IDCA@AgNP solution also reflects the result of detection (Figure 4a, left top). Addition of Zn^{2+} in IDCA@AgNPs resulted in a high aggregation at pH 4−10; simultaneously, a new band appeared. At pH > 10, immediate decolorization of IDCA@AgNPs occurred, and the band disappeared because of the formation of colloidal $Zn(OH)_2$.[32] At pH < 3, similar change was observed because in more acidic conditions the competition between H^+ and Zn^{2+} ions with the free carboxylic groups of IDCA@AgNPs rendered the aggregation of IDCA@AgNPs. Therefore, the optimal pH range for detecting Zn^{2+} by IDCA@AgNPs is 3−10 (Figure 4). Almost similar trends followed when Hcy was added (1 μM) onto IDCA@AgNPs at different pH (Figure 4). However, the suitable pH range for the

https://doi.org/10.1021/acsomega.2c04165
ACS Omega 2022, 7, 33423−33431

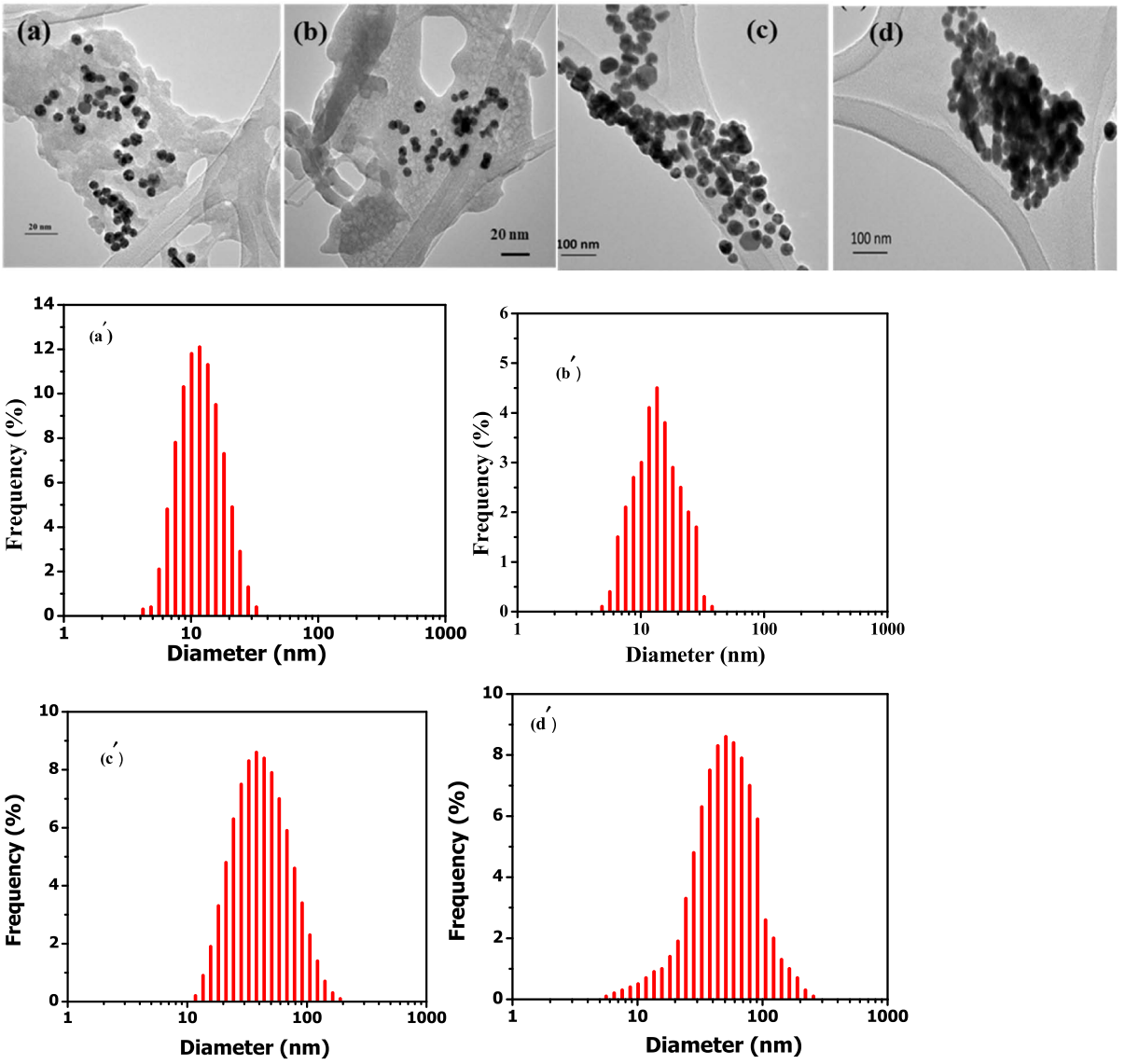

Figure 3. TEM images and their corresponding DLS of citrate@AgNPs (a,a′), IDCA@AgNPs (b,b′), IDCA@AgNPs-Zn^{2+} (c,c′), and IDCA@AgNPs-Hcy (d,d′).

detection of Hcy is 4−9, and the color of the IDCA@AgNP solution also reflects the result of detection (Figure 4, top, right).

3.3. Sensitivity of IDCA@AgNPs toward Zn^{2+} and Hcy.

The sensing ability of IDCA@AgNPs with metal ions and various amino acids in aqueous solutions was tested. To evaluate the selectivity of IDCA@AgNPs toward various metal ions and various amino acids, the UV−vis absorption spectra of IDCA@AgNPs were observed in the presence of several metal ions (Zn^{2+}, Cr^{3+}, Hg^{2+}, Cd^{2+}, Pb^{2+}, Cu^{2+}, Ni^{2+}, Co^{2+}, Fe^{2+}, Fe^{3+}, Ca^{2+}, Mg^{2+}, K^{+}, and Na^{+}) and various amino acids (Hcy, Cys, Glu, Asp, Gly, His, Try, Lys, Ala, Cret, Theo, Phy-ala, Ser, and Met). Figure 5 shows the effect of metal ions on the appearance of IDCA@AgNPs in solution. Zn^{2+} was the only ion that resulted in an absorption peak shift from 397 to 482 nm. This red shift could also be observed by the naked eye as a color change from yellow to red. Other metal ions did not influence the absorption spectra, indicating that no aggregation occurred. Thus, IDCA@AgNPs showed excellent sensitivity to Zn^{2+} ion over different metal ions. On the other hand, we tested the sensing ability of IDCA@AgNPs toward various amino acids such as Hcy, Cys, Glu, Asp, Gly, His, Try, Lys, Ala, Cret, Theo, Phy-ala, Ser, and Met. Figure 6 shows the effect of amino acids on the appearance of IDCA@AgNPs in solution. Hcy was the only ion that resulted in an absorption peak shift from 397 to 512 nm. This red shift could also be observed by the naked eye as a color change from yellow to red. Other amino acids did not influence the absorption spectra, indicating that no aggregation occurred. Thus, IDCA@AgNPs detect Zn^{2+} and Hcy from aqueous solution.

For addressing the sensitivity of the colorimetric assay, we choose two different wavelengths (for Zn^{2+}: 397 and 485 nm; and for Hcy: 397 and 512 nm). The inset of Figure 7 shows a linear relationship (R^2 = 0.97743) between the absorption ratios (A_{485}/A_{397}) of IDCA@AgNPs with the concentration of Zn^{2+} over the range from 1 to 500 μM. From Figure 7, it is evident that the degree of aggregation of IDCA@AgNPs depends on the concentration of Zn^{2+} ions. The absorption spectra changed with the addition of different concentrations of Zn^{2+}, and the change of color of IDCA@AgNPs could also

https://doi.org/10.1021/acsomega.2c04165
ACS Omega 2022, 7, 33423−33431

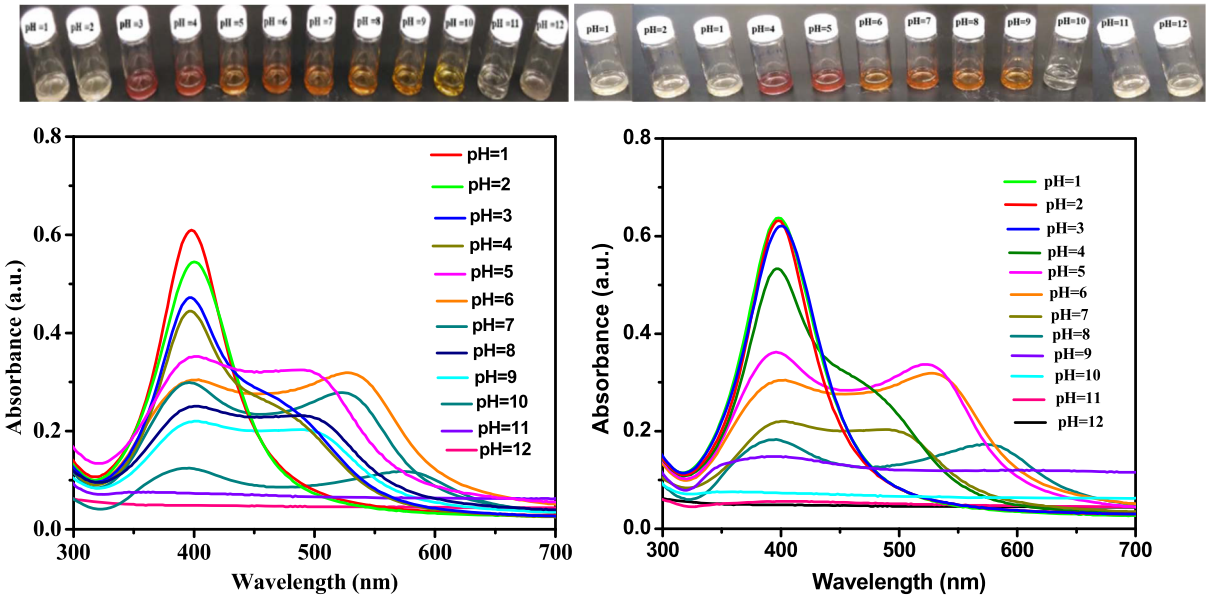

Figure 4. Photographic images (left, top) and absorbance spectra (left, bottom) of IDCA@AgNPs in the presence of Zn^{2+} ion in the pH range 1−12 and photographic images (right, top) and absorbance spectra (right, bottom) of IDCA@AgNPs in the presence of Hcy in the pH range 1−12.

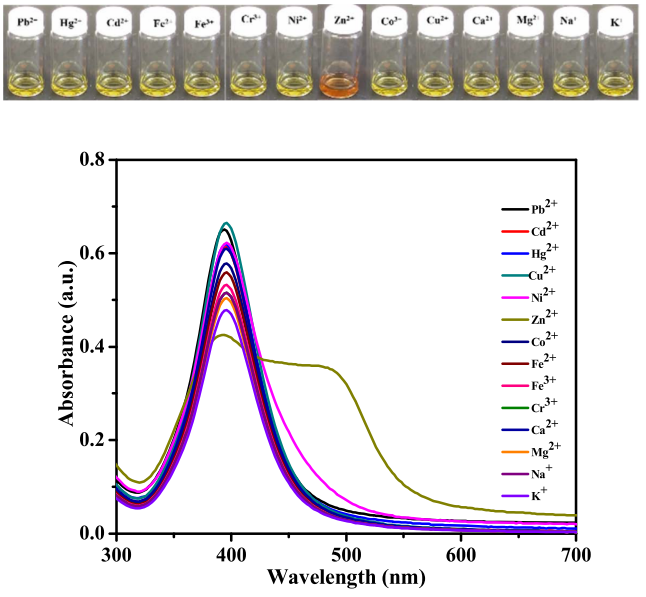

Figure 5. Photographic images (top) and UV−vis spectra (bottom) of IDCA@AgNPs in the presence of different metal ions (50 μM).

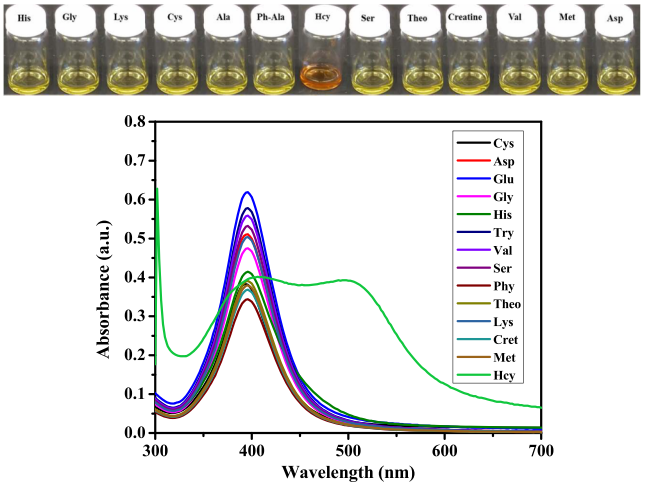

Figure 6. Photographic images (top) and UV−vis spectra (bottom) of AgNPs in the presence of different amino acids (4 μM).

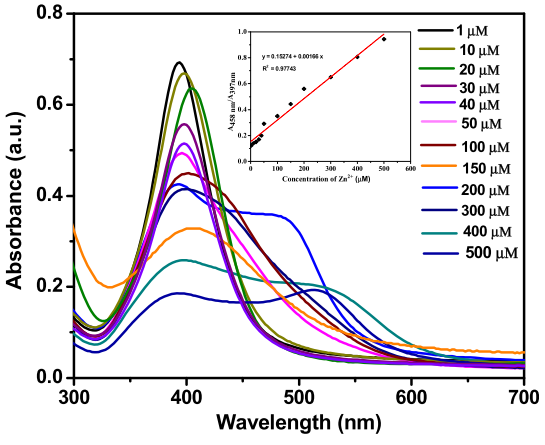

Figure 7. Change of absorption spectra of IDCA@AgNPs in the presence of various concentrations of Zn^{2+} ion (1.0−500 μM).

be determined by naked eye when the concentration of Zn^{2+} ion was 50 μM (Figure S3, Supporting Information). The limit of detection for Zn^{2+} was found to be 2.38 μM (Figure S4, Supporting Information). On the other hand, we developed analytical data for the quantification of Hcy from aqueous solution. As shown in Figure 8, the UV−visible spectra of IDCA@AgNPs show a strong SPR peak at 397 nm; however, it is gradually decreased with the generation of a new SPR peak at 512 nm as the concentration of Hcy increased from 0.1 to 25 μM. Furthermore, the development of the color change from yellow to red depended on the increasing concentrations of Hcy, and the concentration of Hcy at 1 μM could be rapidly determined with the naked eye (Figure S5, Supporting Information). The insert of Figure 8 shows a linear relationship (R^2 = 0.96699) between the absorption ratio (A_{512}/A_{397}) of

https://doi.org/10.1021/acsomega.2c04165
ACS Omega 2022, 7, 33423−33431

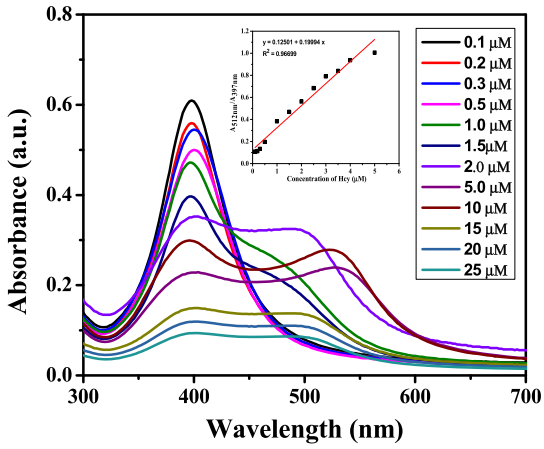

Figure 8. Change of absorption spectra of IDCA@AgNPs in the presence of various concentrations of Hcy (0.1−25 μM).

IDCA@AgNPs and the concentration of Hcy over the range from 0.1 to 25 μM. The limit of detection of Hcy was found to be 0.54 nM (Figure S6, Supporting Information). These results demonstrated that a higher concentration of Hcy induced a higher degree of IDCA@AgNP aggregation. Our work on IDCA@AgNPs is compared with other relevant works (Table S1, Supporting Information), and it is found that our probe (IDCA@AgNPs) is more efficient with respect to other probes.

In order to study the influence of other metal ions on Zn^{2+} binding to IDCA@AgNPs, competitive experiments were carried out in the presence of Zn^{2+} (200 μM) with other metal ions such as Hg^{2+}, Cd^{2+}, Pb^{2+}, Cu^{2+}, Ni^{2+}, Co^{2+}, Fe^{2+}, Fe^{3+}, Cr^{3+}, Ca^{2+}, Mg^{2+}, K^{+}, and Na^{+} at 500 μM (Figure 9). The

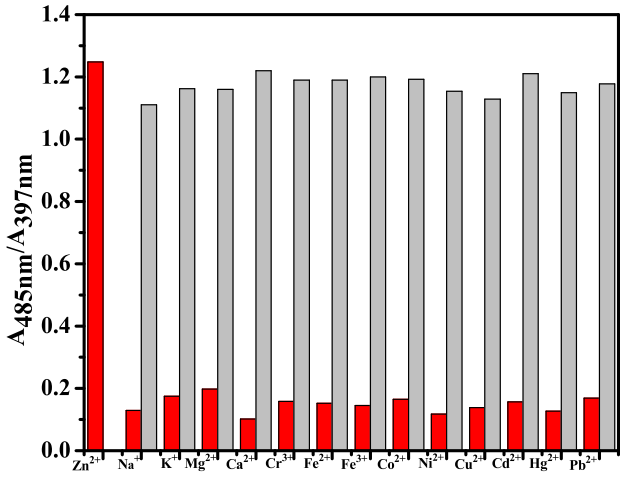

Figure 9. Absorbance ratios (A_{485nm}/A_{397nm}) upon the addition of IDCA@AgNPs to Zn^{2+} for the selected metal ions. Red bars represent the addition of a single metal ion (200 μM), and gray bars are the addition of Zn^{2+} (200 μM) with another metal ion (500 μM).

UV−vis spectra of the above interference ions are shown in Figure S7 (Supporting Information). The SPR absorption shift caused by the mixture of Zn^{2+} with another metal ion was similar to that caused solely by Zn^{2+}. This indicates that other metal ions did not interfere in the binding of IDCA@AgNPs with Zn^{2+}.

On the other hand, we studied the influence of various amino acids on Hcy (4 μM) binding by IDCA@AgNPs; selective experiments were carried out in the presence of several other amino acids such as Cys, Glu, Asp, Gly, His, Try, Lys, Ala, Cret, Theo, Phy-ala, Ser, and Met at 25 μM (Figure 10), and their corresponding UV−vis spectra are shown in

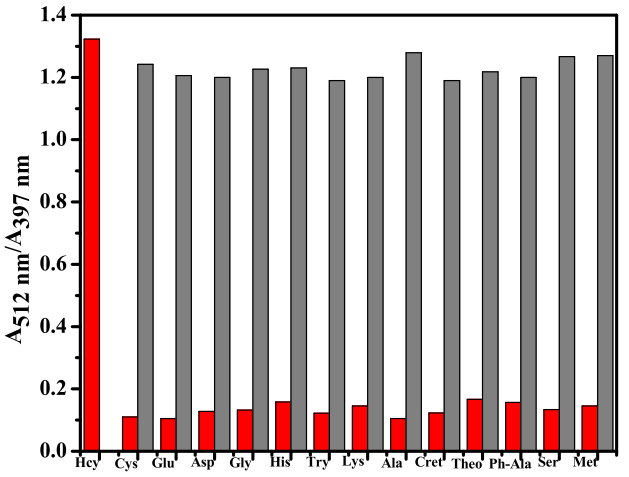

Figure 10. Absorbance ratios (A_{512nm}/A_{397nm}) upon the addition of IDCA@AgNPs to Hcy for the selected amino acids. Red bars represent the addition of a single amino acid (4 μM), and gray bars are the addition of Hcy (4 μM) with other amino acids (25 μM).

Figure S8 (Supporting Information). The SPR absorption shifts caused by the mixture of Hcy with another amino acid were similar to that caused solely by Hcy. This indicates that other metal ions did not interfere in the binding of IDCA@AgNPs with Hcy.

3.4. Sensing Mechanism for Binding Zn^{2+} and Hcy. To evaluate the sensing mechanism by IDCA@AgNPs toward Zn^{2+} and Hcy, a proposed schematic illustration is shown in Scheme 2. It is evident (Scheme 2) that in IDCA@AgNPs there are two types of binding groups which are imidazole nitrogen and carboxylic group of IDCA. However, it is clearly noticed (Figures 1 and 2) that the nitrogen atom of the imidazole group is utilized for the surface modification of citrate@AgNPs. Thus, in the presence of the deprotonated acidic group (COO^{-}) of IDCA, both Zn^{2+} and Hcy can bind simultaneously, resulting in the different aggregation of IDCA@AgNPs in solution, changing the color from yellow to red. To clarify the involvement of the COO^{-} group for simultaneously binding with Zn^{2+} and Hcy, FTIR spectra were recorded by mixing Zn^{2+} (200) and Hcy (2 μM) onto IDCA@AgNPs and are shown in Figure S9 (Supporting Information). Figure S9 clearly indicates that the original FTIR peak position of the carboxylic group in IDCA@AgNPs (Figure 2) was 1601 cm^{-1} in the absence of Zn^{2+} as well as Hcy. However, in the presence of Zn^{2+} and Hcy, the peak position shifted to 1578 and 1552 cm^{-1} for Zn^{2+} and Hcy, respectively. The binding of Hcy may be due to the participation of carboxylate oxygen of IDCA through the weak hydrogen-bonding interaction with the free −SH group of Hcy. These results support the simultaneous binding of Zn^{2+} and Hcy through the carboxylate oxygen of IDCA@AgNPs. For the further confirmation of binding with Zn^{2+} and Hcy simultaneously, UV−vis spectra were obtained by mixing Zn^{2+} (200 μM) and Hcy (2 μM) solutions onto IDCA@AgNPs, and the results are shown in Figure S10 (Supporting Information). As evident from Figure S10, two peaks at around 485 nm (for Zn^{2+}) and around 512

https://doi.org/10.1021/acsomega.2c04165
ACS Omega 2022, 7, 33423−33431

Scheme 2. Proposed Schematic Illustration for the Simultaneous Detection of Zn^{2+} and Hcy Based on the Aggregation of IDCA@AgNPs

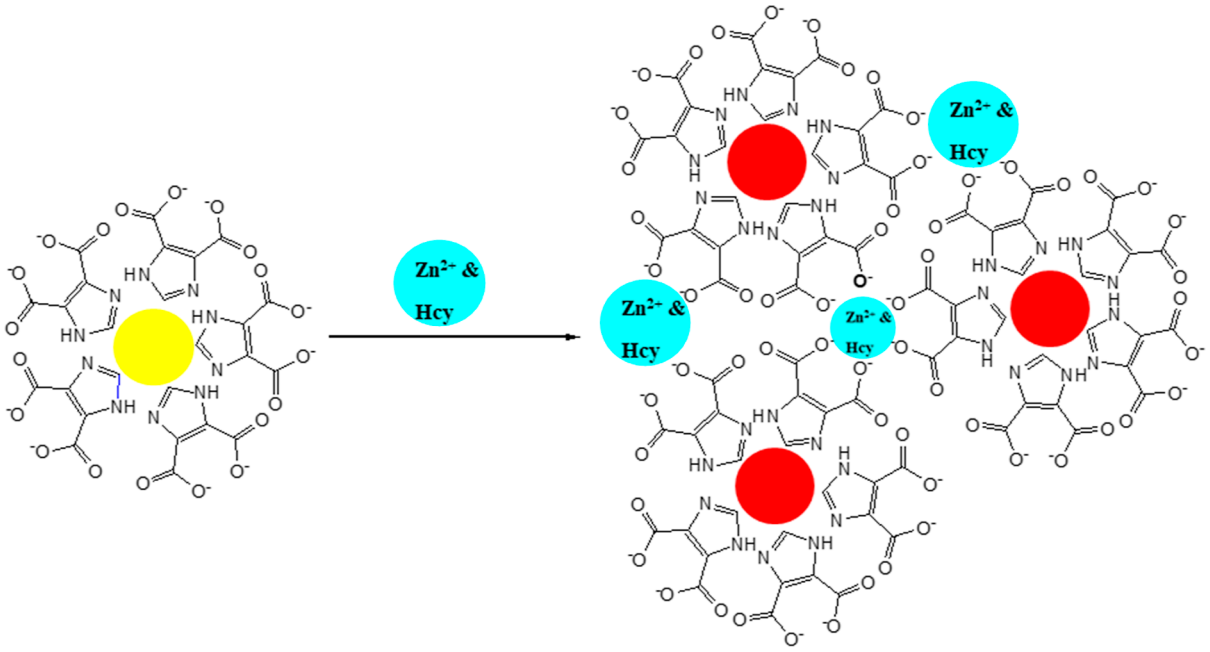

nm (for Hcy) are found as well as the peak of IDCA@AgNPs at 397 nm.

3.5. Application of IDCA@AgNPs for Lake Water Samples and Human Urine. To confirm the practical application of IDCA@AgNPs, water samples were collected from the lakes located in Tempe, Arizona, USA. All water samples were filtered through a 0.2 μm membrane and then spiked with different amounts of Zn^{2+}. In the case of Hcy, human urine samples were collected and filtered through a 0.2 μm membrane and then spiked with different amounts of Hcy. A calibration curve of IDCA@AgNPs SPR shifts in the presence of different Zn^{2+} and Hcy concentrations was prepared. The analytical results are shown in Table S2. The results obtained with IDCA@AgNPs were in good agreement with those obtained using the inductively coupled plasma mass spectrometry (ICP−MS) method, with the relative error of less than 2 and 3% for Zn^{2+} and Hcy, respectively. These results indicate that the designed probe is applicable for Zn^{2+} and Hcy detection in water samples.

4. CONCLUSIONS

In summary, a simple, selective, cost-effective, and rapid colorimetric assay for the simultaneous detection of Zn^{2+} and Hcy using IDCA@AgNPs has been explored in this work. Two analytes, Zn^{2+} and Hcy, of a solution, could be monitored by the color change of the IDCA@AgNP probe simultaneously. The reported probe (IDCA@AgNPs) showed good selectivity for Zn^{2+} and Hcy over other several metals ions and amino acids, respectively. Zn^{2+} and Hcy successfully induced the aggregation of IDCA@AgNPs via complex formation between the IDCA@AgNPs of free carboxylate group of IDCA and Zn^{2+} and Hcy, yielding a red shift in the SPR peak from 397 to 485 nm (for Zn^{2+} ion) and 397 to 512 nm (for Hcy), accompanied by the color change from yellow to red. Zn^{2+} and Hcy have been detected in the wide ranges of pH (pH 3−10). The prepared probe (IDCA@AgNPs) showed good analytical application of environmental water samples, with the relative errors of 2 and 3% for Zn^{2+} and Hcy, respectively..

■ ASSOCIATED CONTENT

Supporting Information

The Supporting Information is available free of charge at https://pubs.acs.org/doi/10.1021/acsomega.2c04165.

Materials and instrumental details; colorimetric determination of Zn^{2+} and Hcy; lake water and human urine sample analyses for Zn^{2+} and Hcy, respectively; control study of Zn^{2+} and Hcy; photographic images and effects of various pH on IDCA@AgNPs; photographic images at various concentrations of Zn^{2+}; calibration curve of IDCA@AgNPs for Zn^{2+}; photographic images of various Hcy concentrations; calibration curve of IDCA@AgNPs for Hcy; UV−vis spectra of IDCA@AgNPs in the presence of different metal ions; UV−vis spectra of IDCA@AgNPs in the presence of different amino acids; FTIR spectra of IDCA@AgNPs in the presence of both Zn^{2+} and Hcy; UV−visible spectra of IDCA@AgNPs in a mixture of Zn^{2+} and Hcy; comparison of our work with other relevant works; and determination of Zn^{2+} and Hcy in lake water and human urine, respectively (PDF)

■ AUTHOR INFORMATION

Corresponding Authors

Palash Mondal − *School of Molecular Sciences, Arizona State University, Tempe, Arizona 85287-1604, United States;* Present Address: Department of Chemistry (UG &PG), Vivekananda Mahavidyalaya, Burdwan, Purba Bardhaman, West Bengal, 713103, India; orcid.org/0000-0003-0649-1034; Phone: +91-9123942819; Email: palashmondal@vmbdn.ac.in; Fax: (0342)-2646914

Jeffery L. Yarger − *School of Molecular Sciences, Arizona State University, Tempe, Arizona 85287-1604, United States;* orcid.org/0000-0002-7385-5400; Phone: +1 480 399

https://doi.org/10.1021/acsomega.2c04165
ACS Omega 2022, 7, 33423−33431

7705; Email: Jeff.Yarger@proton.me; Fax: (480) 965-2747

Complete contact information is available at: https://pubs.acs.org/10.1021/acsomega.2c04165

Notes

The authors declare no competing financial interest.

■ ACKNOWLEDGMENTS

P.M. thanks UGC, New Delhi, India, for providing financial support in the form of "RAMAN FELLOWSHIP" [Sanctioned no. 5-103/2016(IC), Dated-10-02-2016] and Vivekananda Mahavidyalaya, Burdwan, West Bengal, India, for granting study leave. J.L.Y. acknowledges funding from US DOD Army Research Office under grant no. W911-NF19-10152 and US National Science Foundation Grant (NSF DMR BMAT 1809645).

■ REFERENCES

(1) Roohani, N.; Hurrell, R.; Kelishadi, R.; Schulin, R. Zinc and its importance for human health: An integrative review. *J. Res. Med. Sci.* **2013**, *18*, 144−157.
(2) Chaffee, B. W.; King, J. C. Effect of Zinc Supplementation on Pregnancy and Infant Outcomes: A Systematic Review. *Paediatr. Perinat. Epidemiol.* **2012**, *26*, 118−137.
(3) Noy, D.; Solomonov, I.; Sinkevich, O.; Arad, T.; Kjaer, K.; Sagi, I. Zinc-Amyloid β Interactions on a Millisecond Time-Scale Stabilize Non-fibrillar Alzheimer-Related Species. *J. Am. Chem. Soc.* **2008**, *130*, 1376−1383.
(4) Jacobsen, D. W. Homocysteine and Vitamins in Cardiovascular Disease. *Clin. Chem.* **1998**, *44*, 1833−1843.
(5) Seshadri, S.; Beiser, A.; Selhub, J.; Jacques, P. F.; Rosenberg, I. H.; D'Agostino, R. B.; Wilson, P. W. F.; Wolf, P. A. Plasma Homocysteine as a Risk Factor for Dementia and Alzheimer's Disease. *N. Engl. J. Med.* **2002**, *346*, 476−483.
(6) Brustolin, S.; Giugliani, R.; Félix, T. M. Genetics of Homocysteine Metabolism and Associated Disorders. *Braz. J. Med. Biol. Res.* **2010**, *43*, 1−7.
(7) Kim, J., II; Moon, J. H.; Chung, H. W.; Kong, M. H.; Kim, H. J. Association between Homocysteine and Bone Mineral Density according to Age and Sex in Healthy Adults. *J. Bone Metab.* **2016**, *23*, 129−134.
(8) Ali, M. Preconcentration and Determination of Trace Amounts of Heavy Metals in Water Samples Using Membrane Disk and Flame Atomic Absorption Spectrometry. *Chin. J. Chem.* **2007**, *25*, 640−644.
(9) Li, Z.; Xiang, Yu.; Tong, A. Ratiometric chemosensor for fluorescent determination of Zn2+ in aqueous ethanol. *Anal. Chem. Acta* **2008**, *619*, 75−80.
(10) Singh, P.; Singh, A. K.; Jain, A. K. Electrochemical Sensors for the Determination of Zn2+ Ions Based on Pendant Armed Macrocyclic Ligand. *Electrochem. Acta* **2011**, *56*, 5386−5395.
(11) Bakirdere, S.; Bramanti, E.; D'ulivo, A.; Ataman, O. Y.; Mester, Z. Speciation and Determination of Thiols in Biological Samples using High Performance Liquid Chromatography−Inductively Coupled Plasma-Mass Spectrometry and High-Performance Liquid Chromatography−Orbitrap MS. *Anal. Chem. Acta* **2010**, *680*, 41−47.
(12) Fernández-Menéndez, S.; Fernández-Sánchez, M. L.; Fernández-Colomer, B.; de la Flor St. Remy, R. R.; Cotallo, G. D. C.; Freire, A. S.; Braz, B. R.; Santelli, R. E.; Sanz-Medel, A. Total Zinc Quantification by Inductively Coupled Plasma-Mass Spectrometry and its Speciation and Size Exclusion Chromatography-Inductively Coupled Plasma-Mass Spectrometry in Human Milk and Commercial Formulas: Importance in Infant Nutrition. *J. Chromatogr. A* **2016**, *1428*, 246−254.
(13) Khan, R.; Yokozuka, Y.; Terai, S.; Shirai, N.; Ebihara, E. Accurate determination of Zn in geological and cosmochemical rock samples by isotope dilution inductively coupled plasma mass spectrometry. *J. Anal. At. Spectrom.* **2015**, *30*, 506−514.
(14) Satterfield, M. B.; Sniegoski, L. T.; Welch, M. J.; Nelson, B. C.; Pfeiffer, C. M. Comparison of Isotope Dilution Mass Spectrometry Methods for the Determination of Total Homocysteine in Plasma and Serum. *Anal. Chem.* **2003**, *75*, 4631−4638.
(15) Mondal, P.; Yarger, J. L. Colorimetric Dual Sensors of Metal Ions Based on 1,2,3-Triazole-4,5-Dicarboxylic Acid-Functionalized Gold Nanoparticles. *J. Phys. Chem. C* **2019**, *123*, 20459−20467.
(16) Ihsan, M.; Niaz, A.; Rahim, A.; Zaman, M. I.; Arain, M. B.; Sirajuddin; Sharif, T.; Najeeb, M. Biologically Synthesized Silver Nanoparticle-Based Colorimetric Sensor for the Selective Detection of Zn2+. *RSC Adv.* **2015**, *5*, 91158−91165.
(17) Lee, S.; Nam, Y.-S.; Lee, H.-J.; Lee, Y.; Lee, K.-B. Highly Selective Colorimetric Detection of Zn(II) Ions Using Label-Free Silver Nanoparticles. *Sens. Actuators, B* **2016**, *237*, 643−651.
(18) Karthiga, D.; Anthony, S. P. Selective Colorimetric Sensing of Toxic Metal Cations by Green Synthesized Silver Nanoparticles over a Wide pH Range. *RSC Adv.* **2013**, *3*, 16765−16774.
(19) Bothra, S.; Kumar, R.; Sahoo, S. K. Pyridoxal Derivative Functionalized Gold Nanoparticles for Colorimetric Determination of Zinc(II) and Aluminium(III). *RSC Adv.* **2015**, *5*, 97690−97695.
(20) Li, W.; Nie, Z.; He, K.; Xu, X.; Li, Y.; Huang, Y.; Yao, S. Simple, rapid and label-free colorimetric assay for Zn2+ based on unmodified gold nanoparticles and specific Zn2+ binding peptide. *Chem. Commun.* **2011**, *47*, 4412−4414.
(21) Leesutthiphonchai, W.; Dungchai, W.; Siangproh, W.; Ngamrojnavanich, N.; Chailapakul, O. Selective Determination of Homocysteine Levels in Human Plasma Using a Silver Nanoparticle-Based Colorimetric Assay. *Talanta* **2011**, *85*, 870−876.
(22) Uehara, N. Colorimetric Assay of Homocysteine using Gold Nanoparticles Conjugated with Thermoresponsive Copolymers. *Anal. Method.* **2016**, *8*, 7185−7192.
(23) Huang, C.-C.; Chang, H.-T. Parameters for Selective Colorimetric Sensing of Mercury(II) in Aqueous Solutions Using Mercaptopropionic Acid-Modified Gold Nanoparticles. *Chem. Commun.* **2007**, 1215−1217.
(24) Khan, U.; Niaz, A.; Shah, A.; Zaman, M. I.; Zia, M. A.; Iftikhar, F. J.; Nisar, J.; Ahmed, M. N.; Akhter, M. S.; Shah, A. H. Thiamine-functionalized silver nanoparticles for the highly selective and sensitive colorimetric detection of Hg2+ ions. *New J. Chem.* **2018**, *42*, 528−534.
(25) Battocchio, C.; Meneghini, C.; Fratoddi, I.; Venditti, I.; Russo, M. V.; Aquilanti, G.; Maurizio, C.; Bondino, F.; Matassa, R.; Rossi, M.; Mobilio, S.; Polzonetti, G. Silver Nanoparticles Stabilized with Thiols: A Close Look at the Local Chemistry and Chemical Structure. *J. Phys. Chem. C* **2012**, *116*, 19571−19578.
(26) Böhme, D.; Düpre, N.; Megger, D. A.; Müller, J. Conformational Change Induced by Metal-Ion-Binding to DNA Containing the Artificial 1,2,4-Triazole Nucleoside. *Inorg. Chem.* **2007**, *46*, 10114−10119.
(27) Jana, N. R.; Gearheart, L.; Murphy, C. J. Wet Chemical Synthesis of Silver Nanorods and Nanowires of Controllable Aspect Ratio. *Chem. Commun.* **2001**, 617−618.
(28) Henglein, A.; Giersig, M. Formation of Colloidal Silver Nanoparticles: Capping Action of Citrate. *J. Phys. Chem. B* **1999**, *103*, 9533−9539.
(29) Nakamoto, K. *Infrared and Raman Spectra of Inorganic and Coordination Compounds: Part A: Theory and Applications in Inorganic Chemistry*, 6th ed.; John Wiley & Sons, 2008.
(30) Wang, G. L.; Dong, Y.-M.; Zhu, X.-Y.; Zhang, W.-J.; Wang, C.; Jiao, H.-J. Ultrasensitive and Selective Colorimetric Detection of Thiourea using Silver Nanoprobes. *Analyst* **2011**, *136*, 5256−5260.
(31) Abargues, R.; Albert, S.; Valdés, J. L.; Abderrafi, K.; Martínez-Pastor, J. P. M. Molecular-Mediated Assembly of Silver Nanoparticles with Controlled Interparticle Spacing and Chain Length. *J. Mater. Chem.* **2012**, *22*, 22204−22211.

(32) Reichle, R. A.; McCurdy, K. G.; Hepler, L. G. Zinc Hydroxide: Solubility Product and Hydroxy-Complex Stability Constants from 12.5-75°C. *Can. J. Chem.* **1975**, *53*, 3841−3845.

https://doi.org/10.1021/acsomega.2c04165
ACS Omega 2022, 7, 33423−33431